ATMOSPHERIC AND OCEANIC SCIENCE LETTERS, 2012, VOL. 5, NO. 5, 389–393

Estimating the Predictability of the Quasi-Biweekly Oscillation Using the Nonlinear Local Lyapunov Exponent Approach

SHI Zhen[1,2] and DING Rui-Qiang[1]

[1] *State Key Laboratory of Numerical Modeling for Atmospheric Sciences and Geophysical Fluid Dynamics (LASG), Institute of Atmospheric Physics, Chinese Academy of Sciences, Beijing 100029, China*
[2] *Graduate University of Chinese Academy of Sciences, Beijing 100049, China*

Received 22 March 2012; revised 2 May 2012; accepted 3 May 2012; published 16 September 2012

Abstract The quasi-biweekly oscillation (QBWO) is a major intraseasonal variability (ISV) in the tropics. Based on bandpass-filtered outgoing longwave radiation (OLR) and wind field data, the predictability limits of the QBWO in boreal summer and boreal winter are investigated using the nonlinear local Lyapunov exponent (NLLE) approach. The analysis shows that the evolution of the mean error growth of the QBWO in boreal summer and the evolution of the mean error growth in boreal winter are comparable. Both curves exhibit rapid growth in the initial stage followed by a slowly fluctuating, ascending trend before saturation is reached. As a result, the potential predictability limits for the boreal summer QBWO are very close to those for the boreal winter QBWO, with a lead time of approximately three weeks. Given the current limitations in the simulation and prediction of ISV, including the QBWO, the results of this study provide a useful reference for assessing the predictability of the QBWO using model simulations.

Keywords: QBWO, EOF, predictability, NLLE
Citation: Shi, Z., and R.-Q. Ding, 2012: Estimating the predictability of the Quasi-Biweekly Oscillation using the nonlinear local Lyapunov exponent approach, *Atmos. Oceanic Sci. Lett.*, **5**, 389–393.

1 Introduction

The tropical atmospheric intraseasonal variability (ISV) contains two distinct bands with 10–20-day (quasi-biweekly oscillation, also known as QBWO) periods and 30–60-day (Madden-Julian oscillation, also known as MJO) periods. The MJO was first discovered by Madden and Julian (1971, 1972), and the QBWO has been observed in spectral analyses of precipitation and horizontal wind records by several authors (Murakami and Frydrych, 1974; Krishnamurti and Ardanuy, 1980; Yasunari, 1981; Chen and Chen, 1993). Given the importance of the ISV in synoptic and climate systems, much work has been devoted to the research of low-frequency oscillations, including the following studies: (1) the structure, propagation, and life cycle of the ISV (Chen and Chen, 1993, 1995; Kiladis and Wheeler, 1995; Numaguti, 1995; Lo and Hendon, 2000; Mao and Chan, 2005); (2) the origin and maintenance mechanism of the ISV (Goswami and Shukla, 1984; Keshavamurthy et al., 1986; Nanjundiah et al., 1992; Chatterjee and Goswami, 2004; Kikuchi and Wang, 2009); (3) the influence of the ISV on the local weather and climate as well as on the global atmospheric circulation, including tropical cyclone formation, and the active/break cycles of both the Indian summer monsoon and the South China Sea monsoon (Fukutomi and Yasunari, 1999; Annamalai and Slingo, 2001; Zhu et al., 2004; Goswami, 2005; Li and Wang, 2005; Li and Zhou, 2009; Wang et al., 2009; He et al., 2011); and (4) the predictability limit of the ISV (Goswami and Xavier, 2003; Fu et al., 2007; Jiang et al., 2008; Seo et al., 2009; Ding et al., 2010, 2011).

Most of the existing work related to the ISV focuses on the MJO. By comparison, many aspects of the QBWO have not been fully considered. In particular, estimates of the predictability limit remain elusive. Although the predictability of the MJO has been rigorously examined using models and observations, the predictability of the QBWO still remains an open issue and needs to be explored. The objective of this paper is to estimate the predictability limit of the QBWO using two decades of observations.

2 Data and methods

The data used in this study include outgoing longwave radiation (OLR) and 850 hPa wind fields. The OLR data are daily averaged values from the National Oceanic and Atmospheric Administration (NOAA), which can be used as a proxy for tropical convective activity (Waliser et al., 1993; Liebmann and Smith, 1996). The 850 hPa wind data are from the National Centers for Environmental Prediction-National Center for Atmospheric Research (NCEP-NCAR) reanalysis (Kalnay et al., 1996). Both the OLR and 850 hPa winds are analyzed on a 2.5° latitude× 2.5° longitude grid for the period 1979–2010.

To extract the QBWO signal, the seasonal cycle is removed from the datasets by subtracting the time series mean and the first three harmonics of the annual cycle, leaving the anomalies. Then, a 10–20-day bandpass Lanczos filter is applied to the anomalies before performing a combined empirical orthogonal function (EOF) of the OLR and 10–20-day filtered zonal and meridional winds at 850 hPa.

To estimate the predictability limit of chaotic systems, Ding and Li (2007) introduced a new approach using the nonlinear local Lyapunov exponent (NLLE). By develop-

Corresponding author: DING Rui-Qiang, drq@mail.iap.ac.cn

ing an algorithm that yields estimates of the NLLE and its derivatives using observational data, the potential predictability limits of weather and climate events can be determined (Li and Wang, 2008; Ding and Li, 2009; Ding et al., 2010, 2011; Li and Ding, 2011). In this study, this method is applied to produce the estimated predictability of the QBWO.

3 Results and discussion

Figure 1 shows the geographical distribution of the QBWO in the tropical region during boreal summer (1 May to 30 September) and boreal winter (1 November to 31 March). The standard deviation of the 10–20-day filtered data exhibits different features in different seasons (Figs. 1a and 1b). For instance, in boreal summer, the standard deviation displays the highest values in the Asian summer monsoon area. However, in boreal winter, the region with the highest standard deviations is located to the east of the Australian continent in the Southern Hemisphere. Figures 1c and 1d show the percent variance of the 10–20-day band relative to the variance of the unfiltered data are shown in Figs. 1c and 1d for summer and winter, respectively. These data illustrate the convective activity associated with the QBWO. In general, the prominent convective signal lies in the subtropical regions between 10° and 30° latitude in both hemispheres. These features are consistent with the geographical distribution of the QBWO convection identified by Kikuchi and Wang (2009). Based on the above findings, different regions are selected for boreal summer and boreal winter for input to the EOF analysis. For boreal summer, the region is confined to 10°S–30°N and 40°E–120°E, while for boreal winter, the region is confined to 30°S–10°N and 120°E–160°W. A combined EOF analysis of OLR anomalies and 10–20-day filtered zonal and meridional winds at 850 hPa is carried out for these regions.

Figures 2 and 3 indicate the spatial structures of the two leading EOFs for the combined filtered OLR and 850 hPa winds during boreal summer and boreal winter, respectively. According to the criteria proposed by North et al. (1982), the first two EOFs are well separated from the remaining EOFs and contain the dynamic signal for both the boreal summer and boreal winter. The two principal EOFs depict the horizontal structure and westward propagation of the QBWO during boreal summer (Figs. 2a and 2b). For EOF1, enhanced convection is evident over the South China Sea and the Bay of Bengal, while reduced convection is mainly located over the north Indian Ocean and South China. The double vortex structure accompanied by enhanced convection can clearly be seen. For EOF2, enhanced convection moves westward into the Indian Ocean, while reduced convection occurs over the South China Sea. The associated double vortex structure also moves westward. The principal components (PC) time series shows the time-varying amplitude of the EOF spatial structure. A subset of the PC time series (boreal summer of 1989) is shown in Fig. 2c. PC 1 leads PC 2 by approximately four days, which is equivalent to a quarter of a cycle and consistent with the westward propagation of the QBWO.

For boreal winter, the two principal EOFs display enhanced convection over northeast Australia (Figs. 3a and 3b). In EOF1, enhanced convection is present to the northeast of Australia, while reduced convection appears in the area near the dateline. In EOF2, enhanced convection can be found in the area around the dateline and the equatorial west Pacific. Both modes have a double vortex structure with a stronger vortex located in the Southern Hemisphere. PC 1 lags PC 2 by approximately a quarter of a cycle, which indicates the westward propagation of the QBWO.

All of these structures are in agreement with the results of previous research (e.g., Chen and Chen, 1993; Goswami and Ajaya, 2001; Mao and Chan, 2005; Wen et al., 2011). This agreement suggests that the main characteristics of the QBWO in boreal summer and boreal winter are captured by the two principal EOFs. As noted by Ding et al. (2011), the vector $\boldsymbol{Z}$ in the two-dimensional phase space consists of the first two PCs and can represent the MJO. $\boldsymbol{Z}$ is defined by the following (t is the time):

$$\boldsymbol{Z}(t) = [\mathrm{PC1}(t),\ \mathrm{PC2}(t)]. \quad (1)$$

The mean error growth of $\boldsymbol{Z}$ can then be calculated using the NLLE approach. Similarly, the predictability of QBWO in boreal summer and boreal winter can be obtained by applying this method. Figures 4a and 4b show

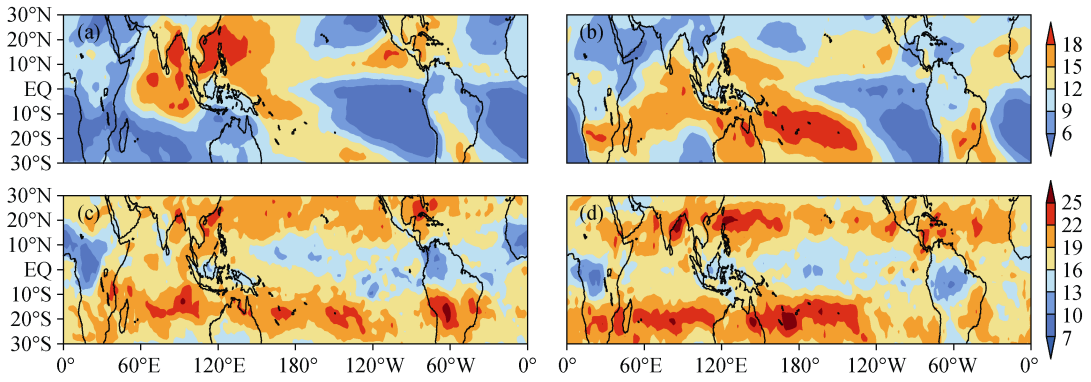

Figure 1 Geographical distribution of the standard deviation of the 10–20-day filtered OLR in the tropical region during (a) boreal summer and (b) boreal winter. Also shown is the percent variance explained by the 10–20-day band relative to the unfiltered variance for (c) boreal summer and (d) boreal winter. Shaded intervals are 3 W m^{-2} in (a) and (b), and 3% in (c) and (d).

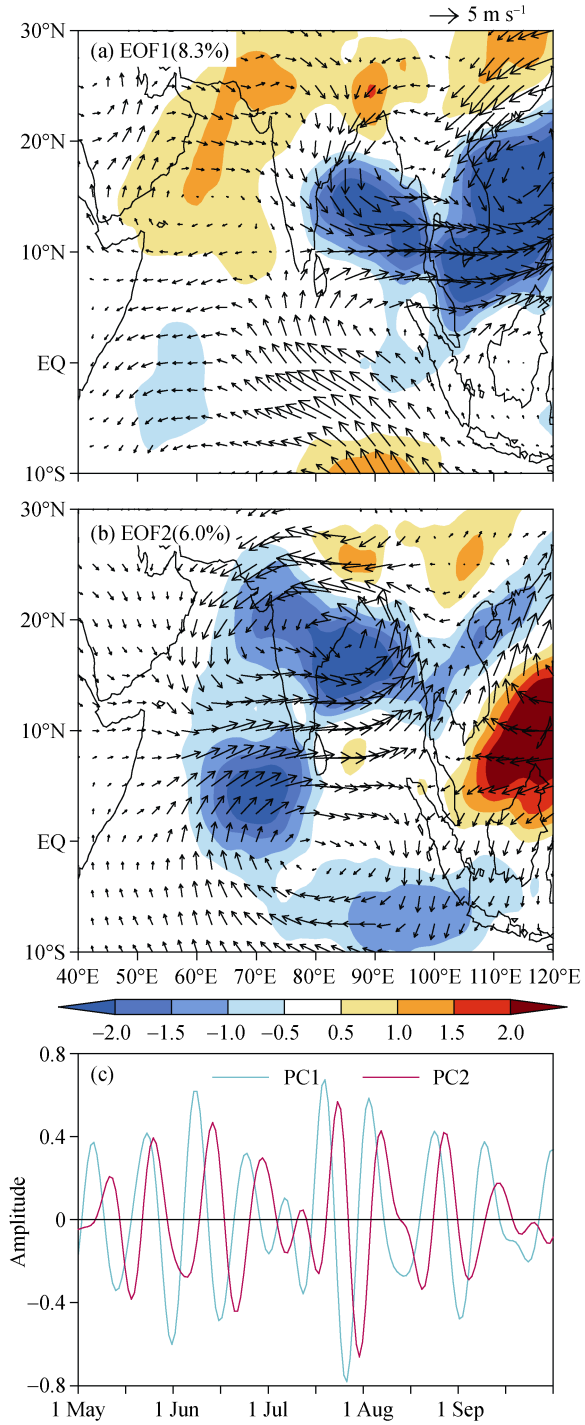

Figure 2 EOF analysis for the combined fields of 10–20 day filtered OLR (W m^{-2}) and 850 hPa winds (m s^{-1}) during boreal summer: (a) EOF1, (b) EOF2, and (c) PC1 and PC2 for the period 1 May 1989 to 31 September 1989.

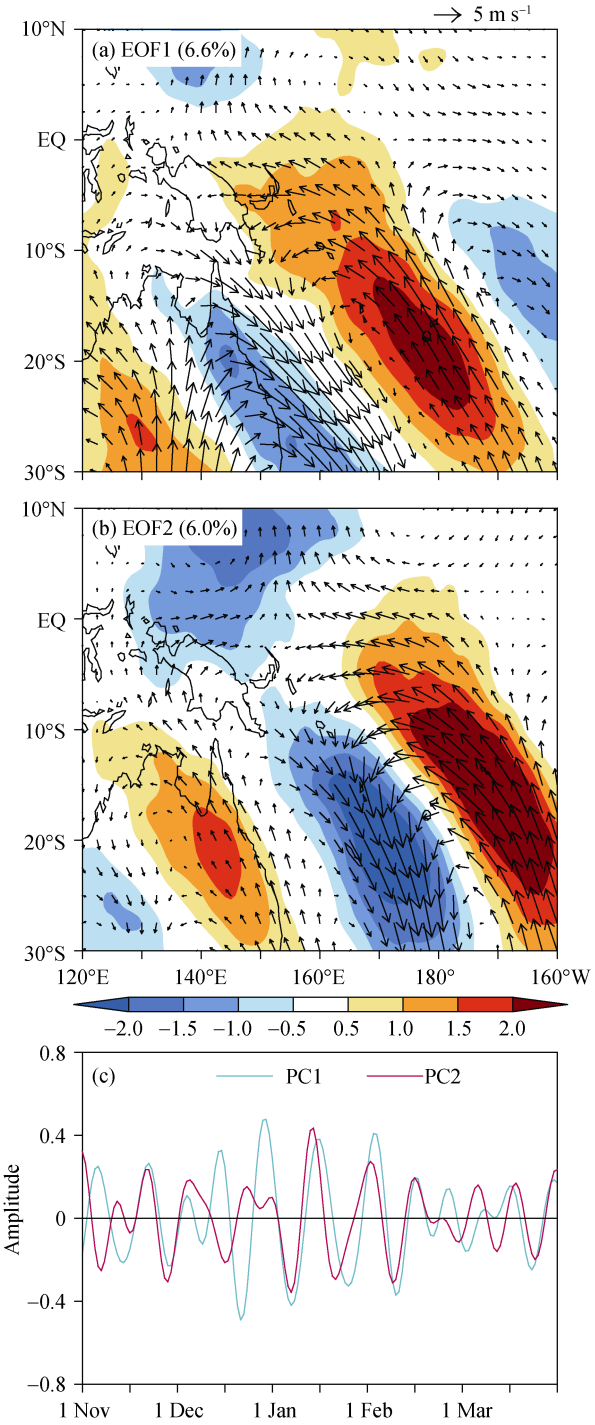

Figure 3 EOF analysis for the combined fields of 10–20-day filtered OLR (W m^{-2}) and 850 hPa winds (m s^{-1}) during boreal winter: (a) EOF1, (b) EOF2, and (c) PC1 and PC2 for the period 1 November 1989 to 31 March 1990.

the mean error growth of ***Z*** in boreal summer and boreal winter, respectively. In both seasons, the mean error of ***Z*** shows a rapid initial increase followed by a relatively slow, fluctuating growth before the saturation level is reached. Following Ding et al. (2011), the mean error growth of the QBWO implies that different time scales determine different phases of error growth. In the first week, the initial conditions exert a large influence on the mean error growth of the QBWO. After this phase, the slowly varying boundary conditions, as coupled convective phenomenon, begin to play a more important role in determining the mean error growth of the QBWO. The mean error growth continues to fluctuate until the saturation level is reached. Compared with results for the MJO (Ding et al., 2010, 2011), the slowing growth stage of the QBWO is short but exhibits greater variability. This may

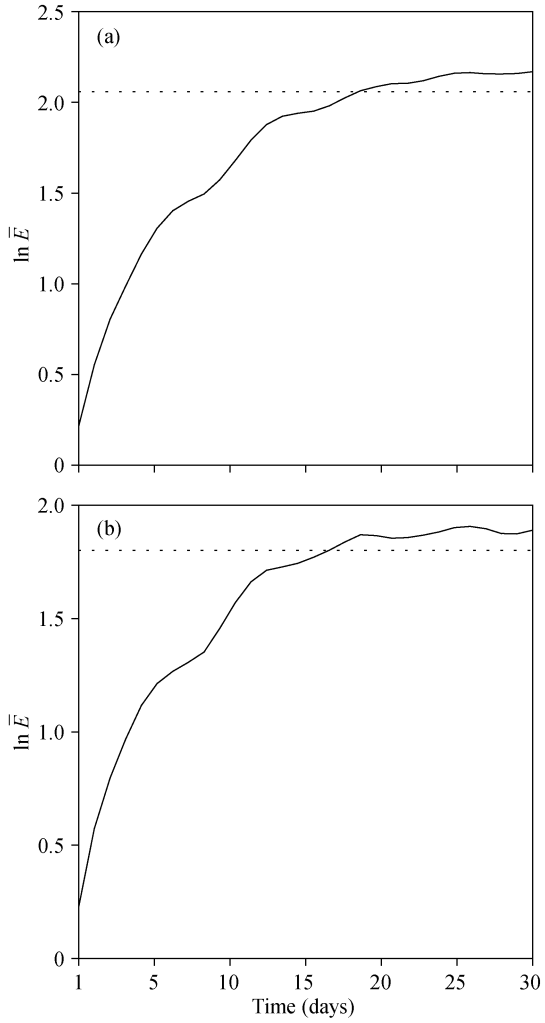

Figure 4 (a) Mean error growth of the vector ***Z*** in the two-dimensional phase space defined by the first two PCs derived from the EOF analysis of the combined filtered OLR and 850 hPa winds during boreal summer (MJJAS). (b) Same as (a), but the mean error growth of the vector ***Z*** during boreal winter (NDJFM) is shown. $\bar{E}$ denotes the mean error of the vector ***Z***. The dashed line represents the 95% level of the saturation.

be attributed to the smaller scale of the QBWO in contrast to that of the MJO. As the potential predictability limit is defined as the time at which the error reaches 95% of its saturation level, Figs. 4a and 4b suggest that the potential predictability of QBWO in boreal summer and winter is 21 and 22 days, respectively. Previous studies have noted that the spatio-temporal characteristics of boreal summer and boreal winter are very similar (Chatterjee and Goswami, 2004), which correspond to the similar potential predictability limits found in the present study for the two seasons.

Existing models often underestimate the inherent limits of prediction for the ISV because of limitations in, for example, simulating ocean-atmosphere interactions, adapting to arbitrary conditions, and taking advantage of known physical constraints (Chen and Alpert, 1990; Lau and Chang, 1992; Kirtman et al., 1997; Fu et al., 2003). Thus, these models are only capable of providing information captured by the initial conditions of the earth systems, leading to an underestimation of the ISV. Figures 4a and 4b indicate that the early phases of error growth of the QBWO in boreal summer and boreal winter, unlike those of tropical intraseasonal variability (Ding et al., 2011), have a comparable growth rate. This is most likely because a universal mechanism governs genesis and scale selection of the boreal summer and boreal winter QBWO (Chatterjee and Goswami, 2004). The mean error growth of ***Z*** switches to its slower developing stage after approximately one week in both boreal winter and boreal summer. This trend may indicate that the predictability of the QBWO in both seasons is influenced mainly by the initial conditions and is therefore limited to approximately one week. As such, existing models may reflect this short timeframe and produce low estimates of the predictability of the QBWO. Research into the predictability of the QBWO estimated by models is still in its infancy, and therefore, the results of the present study offer a useful reference for future modeling studies.

4 Conclusions

This paper examines the two principal EOF modes of the QBWO for boreal summer and boreal winter. Both modes depict the horizontal structure and westward propagation of the QBWO. Using the two PCs, the predictabilities of the QBWO in boreal summer and boreal winter are determined by the NLLE method. The results show that the potential predictability limit of the QBWO is 21 and 22 days for boreal summer and boreal winter, respectively. For both seasons, the mean error growth of the QBWO in different phases shows a consistent development. The results presented here provide a useful reference for model simulations of the QBWO.

Some issues remain unresolved. For example, as the atmospheric predictability is largely a function of space (Kumar et al., 2003; Reichler and Roads, 2004), how do the spatial distributions of the potential predictability limits of the QBWO in boreal summer and boreal winter vary? Do different phases of the life cycle of the QBWO exhibit different patterns of mean error growth? To what extent does the MJO modulate the QBWO in relation to predictability? These problems are worthy of further investigation.

Acknowledgements. This research was funded by the National Natural Science Foundation of China (41175069) and the National Basic Research Program of China (973 program, 2010CB950400).

References

Annamalai, H., and J. M. Slingo, 2001: Active/break cycles: Diagnosis of the intraseasonal variability of the Asian summer monsoon, *Climate Dyn*., **18**, 85–102.

Chatterjee, P., and B. N. Goswami, 2004: Structure, genesis and scale selection of the tropical quasi-biweekly mode, *Quart. J. Roy. Meteor. Soc*., **130**, 1171–1194.

Chen, T. C., and J. C. Alpert, 1990: Systematic errors in the annual and intraseasonal variations of the planetary-scale divergent circulation in NMC medium-range forecasts, *Mon. Wea. Rev*., **118**, 2607–2623.

Chen, T. C., and J. M. Chen, 1993: The 10–20 day mode of the 1979

Indian monsoon: Its relation with time variation of monsoon rainfall, *Mon. Wea. Rev.*, **121**, 2465–2482.

Chen, T. C., and J. M. Chen, 1995: An observational study of the South China Sea monsoon during the 1979 summer: Onset and life cycle, *Mon. Wea. Rev*., **123**, 2295–2318.

Ding, R. Q., and J. P. Li, 2007: Nonlinear finite-time Lyapunov exponent and predictability, *Phys. Lett. A*, **364**, 396–400.

Ding, R. Q., and J. P. Li, 2009: Application of nonlinear error growth dynamics in studies of atmospheric predictability, *Acta Meteor. Sinica* (in Chinese), **67**(2), 241–249.

Ding, R. Q., J. P. Li, and K. H. Seo, 2010: Predictability of the Madden-Julian oscillation estimated using observational data, *Mon. Wea. Rev*., **138**, 1004–1013.

Ding, R. Q., J. P. Li, and K. H. Seo, 2011: Estimate of the predictability of boreal summer and winter intraseasonal oscillations from observations, *Mon. Wea. Rev*., **139**, 2421–2438.

Fu, X. H., B. Wang, T. Li, et al., 2003: Coupling between northward-propagating, intraseasonal oscillations and sea surface temperature in the Indian Ocean, *J. Atmos. Sci*., **60**, 1733–1753.

Fu, X. H., B. Wang, D. Waliser, et al., 2007: Impact of atmosphere-ocean coupling on the predictability of monsoon intraseasonal oscillations, *J. Atmos. Sci*., **64**, 157–174.

Fukutomi, Y., and T. Yasunari, 1999: 10–25 day intraseasonal variations of convection and circulation over East Asia and western North Pacific during early summer, *J. Meteor. Soc*., **77**, 753–769.

Goswami, B. N., 2005: South Asian monsoon, in: *Intraseasonal Variability in the Atmosphere-Ocean Climate System*, W. K. M. Lau and D. E. Waliser (Eds.), Springer, Heidelberg, 19–61.

Goswami, B. N., and M. R. S. Ajaya, 2001: Intraseasonal oscillations and interannual variability of the Indian summer monsoon, *J. Climate*, **14**(6), 1180–1198.

Goswami, B. N., and J. Shukla, 1984: Quasi-periodic oscillations in a symmetric general circulation model, *J. Atmos. Sci.*, **41**, 20–37.

Goswami, B. N., and P. K. Xavier, 2003: Potential predictability and extended range prediction of Indian summer monsoon breaks, *Geophys. Res. Lett*., **30**, 1966, doi:10.1029/2003GL017810.

He, J., H. Lin, and Z. Wu, 2011: Another look at influences of the Madden-Julian Oscillation on the wintertime East Asian weather, *J. Geophys. Res.*, **116**, D03109, doi:10.1029/2010JD014787.

Jiang, X. N., D. E. Waliser, M. C. Wheeler, et al., 2008: Assessing the skill of an all-season statistical forecast model for the Madden-Julian oscillation, *Mon. Wea. Rev*., **136**, 1940–1956.

Kalnay, E., M. Kanamitsu, R. Kistler, et al., 1996: The NCEP/NCAR 40-year reanalysis project, *Bull. Amer. Meteor. Soc*., **77**, 437–471.

Keshavamurthy, R. N., S. V. Kasrure, and V. Krishnakumar, 1986: 30–50 day oscillation of the monsoon: A new theory, *Beitr. Phys. Atmos*., **59**, 443–454.

Kikuchi, K., and B. Wang, 2009: Global perspective of the quasi-biweekly oscillation, *J. Climate*, **22**, 1340–1359.

Kiladis, G. N., and M. Wheeler, 1995: Horizontal and vertical structure of observed tropospheric equatorial Rossby waves, *J. Geophys. Res.*, **100**(D), 22981–22997.

Kirtman, B. P., J. Shukla, B. H. Huang, et al., 1997: Multiseasonal predictions with a coupled tropical ocean-global atmosphere system, *Mon. Wea. Rev*., **125**, 789–808.

Krishnamurti, T. N., and P. Ardunuy, 1980: The 10–20-day westward propagating mode and breaks in the monsoons, *Tellus*, **32**, 15–26.

Kumar, A., S. D. Schubert, and M. S. Suarez, 2003: Variability and predictability of 200-mb seasonal mean heights during summer and winter, *J. Geophys. Res*., **108**, 4169, doi:10.1029/2002JD 002728.

Lau, K. M., and F. C. Chang, 1992: Tropical intraseasonal oscillation and its prediction by the NMC operational model, *J. Climate*, **5**, 1365–1378.

Li J. P., and R. Q. Ding, 2011: Temporal-spatial distribution of atmospheric predictability limit by local dynamical analogues, *Mon. Wea. Rev.*, **139**, 3265–3283.

Li, J. P., and S. Wang, 2008: Some mathematical and numerical issues in geophysical fluid dynamics and climate dynamics, *Commun. Comput. Phys.*, **3**(4), 759–793.

Li, T., and B. Wang, 2005: A review on the western North Pacific monsoon: Synoptic-to-interannual variabilities, *Terr. Atmos. Oceanic Sci.*, **16**, 285–314.

Li, T., and C. Zhou, 2009: Planetary-scale selection of the Madden-Julian Oscillation, *J. Atmos. Sci.*, **66**, 2429–2443.

Liebmann, B., and C. A. Smith, 1996: Description of a complete (interpolated) outgoing longwave radiation dataset, *Bull. Amer. Meteor. Soc*., **77**, 1275–1277.

Lo, F., and H. H. Hendon, 2000: Empirical extended-range prediction of the Madden-Julian oscillation, *Mon. Wea. Rev*., **128**, 2528–2543.

Madden, R. A., and P. R. Julian, 1971: Detection of a 40–50 day oscillation in the zonal wind in the tropical Pacific, *J. Atmos. Sci*., **28**, 702–708.

Madden, R. A., and P. R. Julian, 1972: Description of global-scale circulation cells in the tropics with a 40–50 day period, *J. Atmos. Sci*., **29**, 1109–1123.

Mao, J. Y., and J. C. L. Chan, 2005: Intraseasonal variability of the South China Sea summer monsoon, *J. Climate*, **18**, 2388–2402.

Murakami, T., and M. Frydrych, 1974: On the preferred period of upper wind fluctuations during the summer monsoon, *J. Atmos. Sci*., **31**, 1549–1555.

Nanjundiah, R. S., J. Srinivasan, and S. Gadgil, 1992: Intraseasonal variation of the Indian summer monsoon. Part II: Theoretical aspects, *J. Meteor. Soc. Japan*, **70**, 529–550.

North, G. R., T. L. Bell, R. F. Cahalan, et al., 1982: Sampling errors in the estimation of empirical orthogonal function, *Mon. Wea. Rev*., **110**, 699–706.

Numaguti, A., 1995: Characteristics of 4- to 20-day period disturbances observed in the equatorial Pacific during the TOGA COARE IOP, *J. Meteor. Soc*. *Japan*, **73**, 353–377.

Reichler, T., and J. O. Roads, 2004: Time-space distribution of long-range atmospheric predictability, *J. Atmos. Sci*., **61**, 249–263.

Seo, K. H., W. Wang, J. Gottschalck, et al., 2009: Evaluation of MJO forecast skill from several statistical and dynamical forecast models, *J. Climate*, **22**, 2372–2388.

Waliser, D. E., N. E. Graham, and C. Gautier, 1993: Comparison of highly reflective cloud and outgoing longwave radiation datasets for use in estimating tropical convection, *J. Climate*, **6**, 331–353.

Wang, B., F. Huang, Z. Wu, et al., 2009: Multi-scale climate variability of the South China Sea Monsoon: A review, *Dyn. Atmos. Oceans*, **47**, 15–37.

Wen, M., S. Yang, W. Higgins, et al., 2011: Characteristics of the dominant modes of atmospheric Quasi-Biweekly Oscillation over tropical-subtropical Americas, *J. Climate*, **24**, 3956–3970.

Yasunari, T., 1981: Structure of an Indian summer monsoon system with around 40-day period, *J. Meteor. Soc*. *Japan*, **59**, 336–354.

Zhu, C. W., T. Nakazawa, and J. P. Li, 2004: Modulation of tropical depression cyclone over the Indian-Western Pacific Oceans by Madden-Jullian Oscillation, *Acta Meteor. Sinica* (in Chinese), **62**(1), 42–51.